Multimodal Radiomic Analysis with Full-Field Digital Mammography and Ultrasound-based Breast Imaging

Andrés Felipe Vargas Molano

Thesis to qualify for the Master's Degree in Electronic Engineering

Advisor

Said Pertuz

PhD in Engineering

Co-advisor

Ana Beatriz Ramírez

PhD in Electrical Engineering

Universidad Industrial de Santander

Facultad de Ingenierías Físico-Mecánicas

Escuela de Ingenierías Eléctrica, Electrónica y de Telecomunicaciones

Maestría en Ingeniería Electrónica

Bucaramanga

2023

Agradecimientos

Primeramente, gracias a Dios por el don de la vida y por permitirme culminar una etapa tan importante en mi vida académica. Gracias por su divina provisión y por ser mi consuelo en los momentos de mayor angustia. Gracias a mamá, mi motivación más grande, sin sus palabras de ánimo, no hubiera logrado tantas cosas. Gracias a mis hermanos por motivarme cada día a ser mejor persona. Por último, gracias a la Universidad Industrial de Santander, en especial al grupo de investigación en conectividad y procesamiento de señales (CPS) y a mis directores Said Pertuz y Ana Ramírez, por el acompañamiento brindado durante los últimos años y por la paciencia con la que me guiaron para cumplir con los objetivos de mi tesis de investigación.

"Y todo lo que hagan o digan, háganlo como verdaderos seguidores del Señor Jesucristo, y denle gracias a Dios el Padre por lo que Cristo ha hecho por ustedes." (Colosenses 3:17 TLA).

Andrés Vargas

Contents

List of Tables

List of Figures

Resumen

Título: Análisis radiómico multimodal con mamografía digital de campo completo e imágenes mamarias basadas en ultrasonido[*]

Autor: Andrés Felipe Vargas Molano[**]

Palabras Clave: Análisis radiómico, Cáncer de seno, Análisis multimodal, Ultrasonido, Mamografía.

Descripción: La tomografía computarizada por ultrasonido es una nueva tecnología de imágenes actualmente investigada para la adquisición de imágenes médicas. Ha despertado interés porque es una técnica no invasiva que genera imágenes a partir de la propagación de ondas de ultrasonido a través del tejido, permitiendo así inferir propiedades del tejido de forma indolora y sin radiaciones ionizantes. Sin embargo, el estándar de oro para el cribado del cáncer de seno es la mamografía, a pesar de presentar algunas limitaciones como la alta tasa de falsos positivos y la exposicion a radiación. Aquí, investigamos si la combinación de características radiómicas de ambas modalidades de imágenes Tomografía computarizada por ultrasonido y mamografía puede mejorar el rendimiento en la detección de lesiones mamarias. Realizamos un ensayo in-silico para la detección de lesiones mamarias. Primero, construimos un conjunto de fantomas mamarios virtuales utilizando VICTRE: 58 fantomas con lesiones mamarias y 58 fantomas sin lesiones. Luego, simulamos la adquisición de imágenes de ultrasonido utilizando la técnica de inversión de forma de onda completa y la adquisición de imágenes mamográficas utilizando el software de simulación de imágenes de rayos X MCGPU. Posteriormente, extrajimos un conjunto de características radiómicas de ambas modalidades de imagen. Finalmente, se evaluó el rendimiento del análisis radiómico multimodal para la tarea de detección de lesiones en términos de AUC y se comparó con el uso de una sola modalidad de imagen. En general, la combinación de ambas modalidades mostró mejoras estadísticamente significativas con AUC de 0,88 (IC: 0,82-0,95) en comparación con el uso de una única modalidad de imagen, con AUC de 0,77 (IC: 0,68-0,86) y 0,81 (IC: 0,73-0,89) para mamografía y tomografía computarizada por ultrasonido, respectivamente. La tomografía computarizada por ultrasonido basada en inversión de onda completa mejoró la detección de lesiones mamarias en combinación con la mamografía.

---

[*] Trabajo de Grado

[**] Facultad de Ingenierías Físico-Mecánicas. Escuela de Ingenierías Eléctrica, Electrónica y Telecomunicaciones. Maestría en Ingeniería Electrónica. Director: Said David Pertuz Arroyo. PhD en Ingeniería. Codirector: Ana Beatriz Ramírez Silva. PhD en Ingeniería Eléctrica.

Abstract

Title: Multimodal Radiomic Analysis with Full-Field Digital Mammography and Ultrasound-based Breast Imaging[*]

Author(s): Andrés Felipe Vargas Molano[**]

Key Words: Radiomic analysis, Breast cancer, Multimodal análisis, Ultrasound, Mammography**.**

Description: Ultrasound computed tomography (USCT) is a new imaging technology currently investigated for the acquisition of medical images. It has drawn a lot of interest because it is a non invasive technique that generates images based on the propagation of ultrasound waves through the tissue, thus allowing to infer tissue properties painlessly and without ionizing radiation. However, the gold standard for breast cancer screening is mammography, despite presenting some limitations such as the high rate of false positives and the fact that the patient must undergo radiation. Here, we investigated whether the combination of radiomic features from both USCT imaging modalities and full-field digital mammography (FFDM) can improve performance in detecting breast lesions. We carried out an in-silico trial for breast lesion detection. First, we constructed a set of virtual breast phantoms (VBPs) using VICTRE (United States Food and Drugs Administration): 58 VBPs with breast lesions and 58 VBPs without lesions. Then, we simulated ultrasound image acquisition using the Full-Waveform Inversion technique, and mammographic image acquisition using the MCGPU X-ray imaging simulation software. Subsequently, we extracted a set of radiomic features from both imaging modalities. Finally, the performance of multimodal radiomic analysis for the lesion detection task in terms of AUC was evaluated and compared against using only one imaging modality. Overall, the combination of both modalities showed statistically significant improvements with AUC of 0.88 (CI: 0.82-0.95) compared to using a single imaging modality, with AUCs of 0.77 (CI: 0.68-0.86) and 0.81 (CI: 0.73-0.89) for mammography and USCT, respectively. FWI-based USCT improved the detection of breast lesions in combination with mammography.

---

[*] Master Degree Thesis

[**]Facultad de Ingenierías Físico-Mecánicas. Escuela de Ingenierías Eléctrica, Electrónica y Telecomunicaciones. Master in Electronic Engineering. Advisor: Said Pertuz. PhD in Engineering. Co-advisor: Ana Beatriz Ramírez. PhD in Electrical Engineering.

Introduction

Breast cancer has had very high incidence and mortality rates in women worldwide (Sung et al., 2021), and the burden from breast cancer is predicted to increase in the comming years (Arnold et al., 2022). This has led researchers to focus their efforts on the early detection of this disease (Valdora et al., 2018). In medical imaging, the concept of radiomic analysis has been applied under the hypothesis that medical images contain relevant information about the development of a disease that is not conspicuous to the human eye (Conti et al., 2021). The main objective of radiomic analysis is the extraction and analysis of different quantitative features from medical images (Van et al., 2020). These features are typically used to train learning algorithms for different tasks, such as detection, diagnosis or risk assessment. Detection aims at establishing whether or not there is a presence of any anormalities in a patient (Gillies et al., 2020). Diagnosis, which goes a little deeper and in addition to detecting anormalities, seeks to classify anormalities depending on their features (Amrane et al., 2018). The aim of risk assessment is to predict whether a patient is at high or low risk of developing breast cancer at future (Hernandez et al., 2021) (Africano et al., 2020).

Worldwide, gold standard for breast cancer screening is mammography. However, one of the main limitations of this imaging modality is that the attenuation values of the lesions are similar to the attenuation in dense tissue, which means that lesions can be easily hidden in the surrounding tissue, especially in dense breasts (Scheel et al., 2015). It also requires compression of the breast and the use of ionizing radiation. Alternatively, breast ultrasound is commonly used as a complementary examination after the detection of an abnormality on mammography (Scheel et al., 2015). Ultrasound does not require breast compression, is non-invasive, and does not expose the

patient to radiation. In recent years, different emerging ultrasound-based imaging techniques have been studied, such as ultrasound computed tomography (USCT), which is attractive because it allows obtaining images that quantitatively represent acoustic properties (speed of sound, acoustic attenuation, density) from breast tissues (Guasch et al., 2020). A reconstruction technique used to obtain these images is full waveform inversion (FWI). One of the main advantages of FWI methods over other current ultrasound imaging techniques is that it takes advantage of information from the entire recorded field, also incorporating acoustic wave propagation effects such as dispersion, scattering and diffraction (Robins et al., 2021).

In-silico trials have been booming recently, as they allow exploration of techniques that are in early stages of development (Abadi et al., 2020). Ultrasound computed tomography is still in the developmental stage and therefore there are no real databases of images obtained with this imaging modality, so we designed an in-silico trial to evaluate the potential of multimodal radiomic analysis using the novel imaging modality USCT and full-field digital mammography (FFDM) for detection of breast lesions.

There are some works that focus their efforts in the creation of synthetic breast models (phantoms) that resemble real anatomy (Sharma et al., 2019). A project known as VICTRE (Virtual Clinical Trial for Regulatory Evaluation) has aimed to demonstrate that computational modeling can play an important role in the regulatory evaluation of imaging products, and for this purpose they sought to replicate an existing clinical trial in-silico. Currently this project includes the development of Monte Carlo-based simulation of radiographic images, the design of high-resolution virtual anatomical models, research of new imaging modalities based on the analysis of

information encoded in scattered x-rays among others (Badano et al., 2018). VICTRE software has been recently verified and experimentally validated (Badal et al., 2021).

To evaluate the performance of multimodal radiomic analysis, we used an algorithm for the detection of breast lesions based on the radiomic analysis. We first created a synthetic database containing a total of 116 realistic VBPs using VICTRE software tools (section 3.1 Breast phantoms Database3.1 Breast phantoms Database). On the one we simulated the acquisition of the reconstructed speed of sound (SOS) images are obtained from frontal 2D slices of the VBPs (section 3.2.1 Acquisition of SOS reconstructions), on the other hand, we simulate the mammograms acquisition process, including the breast compression and X-rays propagation (MGCPU X-ray image simulation software) stages (section 3.2.2 Acquisition of mammograms). Subsequently, we build a lesion detection algorithm based on radiomic features extracted from SOS images and mammograms (section 3.3 Lesion detection algorithm). Finally, We entered the images to the lesion detection algorithm and measured its performance in terms of the area under ROC curve (AUC) (section 4. Experiments and results). The combination of both modalities showed superior performance with AUC of 0.88 compared to performance using a single imaging modality with AUCs of 0.77 and 0.81 for mammography and USCT, respectively. Finally, a review, discussion and conclusion of the obtained results is made (section 5. Discussion and 6. Conclusions).

1. Objectives

1.1 General objective

To design and implement an algorithm for detection of breast lesions using mammography and ultrasound-based imaging.

1.2 Specific objectives

To generate a database of synthetic breast phantoms.

To generate mammograms and ultrasound-based images.

To implement an image processing pipeline for the extraction of radiomic features from mammograms and ultrasound-based images.

To evaluate the performance of the multimodal radiomic analysis.

2. Previous work

2.1 Multimodal image analysis

The use of medical images as a tool for detection and diagnosis of breast cancer has been the object of study during the last decades. The medical images that have been widely used in diagnostic and detection tasks have been mammography, breast ultrasound and magnetic resonance imaging (Yassin et al., 2018). In the literature there are very few works that study the combination of two imaging modalities for diagnosis and detection of breast cancer. Shainer et al. (2009) evaluated the effect of a computer-aided diagnosis (CADx) system on radiologists' performance in discriminating malignant and benign masses on mammograms and three-dimensional (3D) ultrasound (US) images. Kelly et al. (2010) compared the potential diagnostic of mammography alone versus automated whole breast ultrasound (AWBU) plus mammography. These works involved expert assessment by radiologists, who are in charge of giving the diagnosis or the probability of malignancy of the images. Some reseachers argue that computerized analysis has the potential to increase efficiency by rapidly analyzing large volumes of data and providing objective measurements, which can help to reduce the potential for human error and variability (Wang et al., 2012).

2.2 FWI reconstruction

FWI technique has been widely used in the field of geophysics, since it allows obtaining acoustic parameters of the subsoil (Schward et al., 2020). Recently, researchers have focused their efforts on the application of the FWI technique in the medical field, more specifically image acquisition, under the hypothesis that accurate ultrasound images could be generated, different

works have been developed that study the efficacy of FWI in generating high-resolution images. Especially for the breast and the brain (Taskin et al., 2020) (Lucka et al., 2020). Although many of these works have focused on the optimization of the FWI technique (Kleman et al., 2023), and the appropriate location of ultrasound sources and receivers (Ramirez et al., 2017). No studies have yet been conducted to assess the potential of this technique when using the reconstructed images generated using FWI in diagnostic tasks.

3. Materials and Methods

In this section, we present the creation of the virtual breast phantoms and lesion insertion process, the simulation for the acquisition of USCT images and their reconstruction using FWI. Finally, we present the detection model of breast lesions for each imaging modality and the multimodal radiomic analysis.

3.1 Breast phantoms Database

3.1.1 Generation of digital breast phantoms

Because ultrasound computed tomography is at an early development stage, we adopt virtual trials in order to safely and economically explore these new imaging techniques. These trials are run on virtual databases. For this work, we used VICTRE, a software developed by the FDA. This software allows modeling different VBP by configuring different physiological characteristics, different tissues with a voxel size of 50 µm.

The database was initially composed of 58 phantoms without lesions (*controls group*), according to the distribution of BI-RADS 5.0 classification in a study of breast cancer screning

(Pisano et al., 2005) (see Table 1). For illustration, Figure 1 shows 4 phantoms, one for each type of glandularity.

Table 1

Summary of VBPs generated

BIRADS 5.0 classification *Type of glandularity*	**Phantoms amount** *(%)*	**Mean volumen** *(cm^3)*
A *Predominantly fat*	10	749.1
B *Scattered*	46	497.7
C *Heterogeneously dense*	40	255.7
D *Extremely dense*	4	141.8

Figure 1

Phantoms with different glandularities

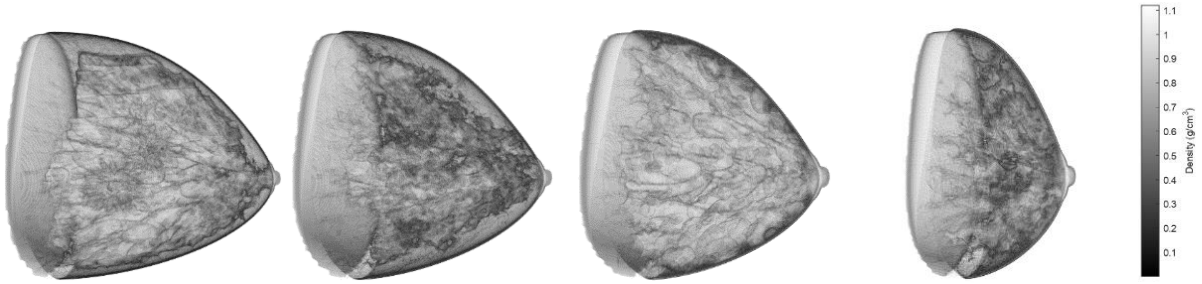

Note. From left to righ: Predominantly fat, Scattered, Heterogeneously dense and Extremely dense.

3.1.2 Lesion Insertion

VICTRE also has an independent pipeline that allows for the generation of spiculated mass lesions. This pipeline uses a Gaussian Random Sphere (GRS) technique to generate a core mass

and an iterative branching algorithm to simulate spicules (De Sisternes et al., 2015). We generated a set of 58 phantoms by inserting spiculated masses with different diameter sizes between 5 mm and 10 mm. Figure 2 shows some examples of spiculated mass lesions. Finally, each lesion was inserted into each phantoms to generate 58 VBPs with lesions (*cases group*). Figure 3 shows the flowchart to generate phantoms without and with lesion.

Figure 2

Spiculated mass phantoms

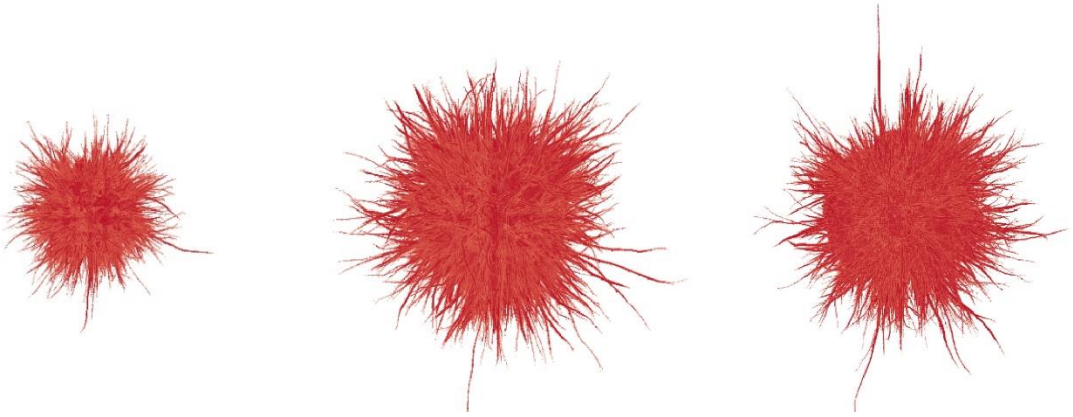

(a) (b) (c)

Note. (a) 5.00mm diameter (b) 7.44mm diameter. (c) 9.64mm diameter.

3.2 Image acquisition

3.2.1 Acquisition of SOS reconstructions

The acquisition process of the SOS reconstructions is divided into two stages: in a first stage, the propagation of acoustic waves emitted by a set of sources is simulated through a two-dimensional sound speed profile (see Figure 4). Table 2 summarizes the speed of sound assigned to each type of tissue. The outside of the breast was filled with water, as it is an ideal medium for

Figure 3

Flowchart to generate the database of VBPs with and without lesión

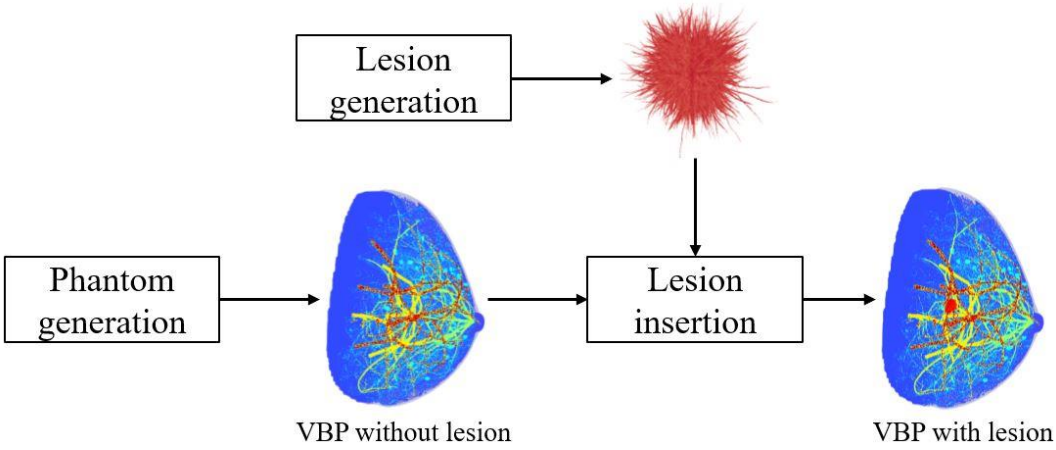

FWI due to its ability to effectively transmit sound waves. In the second stage, the reconstruction of the SOS images is carried out using the FWI technique from the information captured by the receivers.

Table 2

Speed-of-sound (SOS) propagation values for each type of tissue.

Tissue	**Speed-of-sound propagation** *(m/s)*	**Reference**
Fat	1440.0	Hasgal et al., 2012
Glandular	1505.0	Hasgal et al., 2012
Water	1520.0	Ramirez et al., 2017
Ligament	1525.0	Foster et al., 1984
Lesion	1572.0	Foster et al., 1984
Artery	1578.2	Hasgal et al., 2012
Vein	1578.2	Hasgal et al., 2012
Duct	1588.0	Klock et al., 2016
Muscle	1588.4	Hasgal et al., 2012
Nipple	1624.0	Hasgal et al., 2012
Skin	1624.0	Hasgal et al., 2012

Note. Tissues are ordered in increasing value of SOS.

Figure 4

Example of SOS image

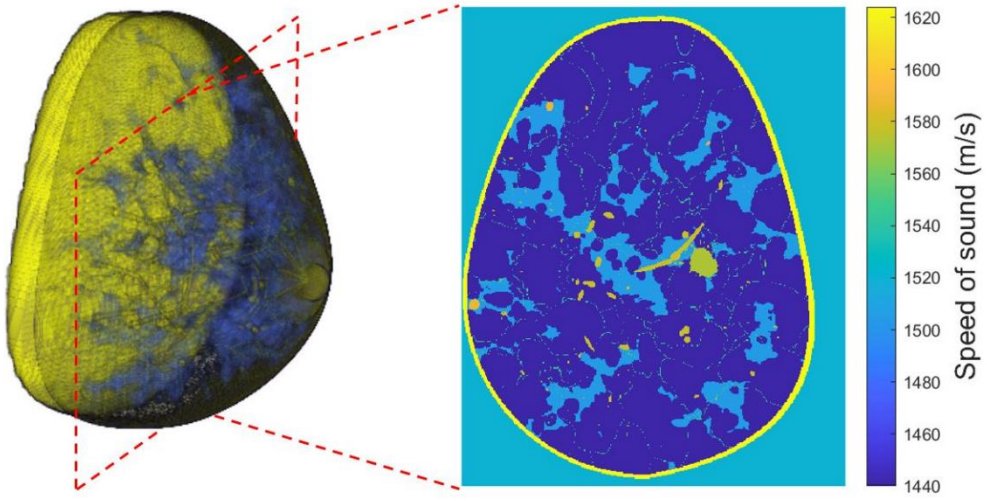

For the FWI reconstruction, we used the Time Domain Inversion (TDI) method, which consists an inverse problem, in which the objective is to reconstruct the unknown speed of the SOS image solving the scalar wave equation with constant density:

$$S_j(x,t) = \frac{1}{c^2(x)}\frac{\partial^2 p_j(x,t)}{\partial t^2} - \nabla^2 p_j \,,$$

where $c(x)$ is the speed of sound profile, $p_j(x)$ represent the time-domain pressure wavefield, $S_j(x,t)$ is the j^{th} source generating the wavefield and t is the time variable.

To find the unknown speed values of the SOS image, FWI seeks to minimize the cost function that measures the mismatch between the modeled data and the observed data. This cost function is given by:

$$\Phi(\mathrm{s}) = ||\mathbf{d}_\mathrm{j}^{\mathrm{mod}} - \mathbf{d}_\mathrm{j}^{\mathrm{obs}}||_{\S}^2 \,,$$

where the $||\cdot||_{\mathbb{S}}^2$ represent the ℓ_2-norm in the data domain, $\mathbf{d}_{\mathrm{j}}^{mod}$ is the modeled data and $\mathbf{d}_{\mathrm{j}}^{obs}$ is the observed data in the spatial domain $\mathbb{S}$.

The modeled data is obtained by using the finite-difference operator $\boldsymbol{\mathcal{R}}\{\cdot\}$ in the time domain:

$$\mathbf{d}_j^{mod} = \boldsymbol{\mathcal{R}}\{\boldsymbol{L}(c)\big[p_j(x,t)\big] + S_j(x,t)\},$$

where

$$\boldsymbol{L}(c)[\cdot] = \nabla^2[\cdot] - \frac{1}{c^2(x)}\frac{\partial^2[\cdot]}{\partial t^2},$$

is the d'Alembertian operator. The update of the speed model is given by the Gauss-Newton method, using the first two terms of the Taylor derivative around the speed model of the previous iteration, thus:

$$c^{n+1} = c^n - \alpha[\mathbf{H}(c^k)]^{-1}\boldsymbol{g}(c^k),$$

where $\mathbf{H}(c^k)$ is the Hessian matrix, α represents the step length and $\boldsymbol{g}(c^k)$ is the gradient of cost function using the adjoint state method (Fichtner et al., 2011). In order to reduce the computational cost, the approximation of the products of the Hessian vector is used using the L-BFGS approach, instead of the exact Hessian matrix.

The reconstructions of SOS images were carried out in the phantoms at pixel size of $2\ mm$, for which downsampling was carried out with a bicubic interpolation, and the temporal step size was $\Delta t\ =\ 0.345\ \mu s$. The number of time samples for the time-domain modeling was $Nt\ =\ 1600$. The values of image pixel size ($\Delta_s = 2\ mm$), ($\alpha = 20$) and number of iterations ($n = 10$) were selected based on the performance in preliminary experiments (Ramirez et al., 2016). The position of sources and receivers were established in a ring configuration (see Figure 5). The ring

configuration in FWI for breast imaging is preferred because it allows for a more complete and accurate reconstruction of the breast tissue (Perez et al., 2017).

Figure 5

Ring configuration for sources and receivers

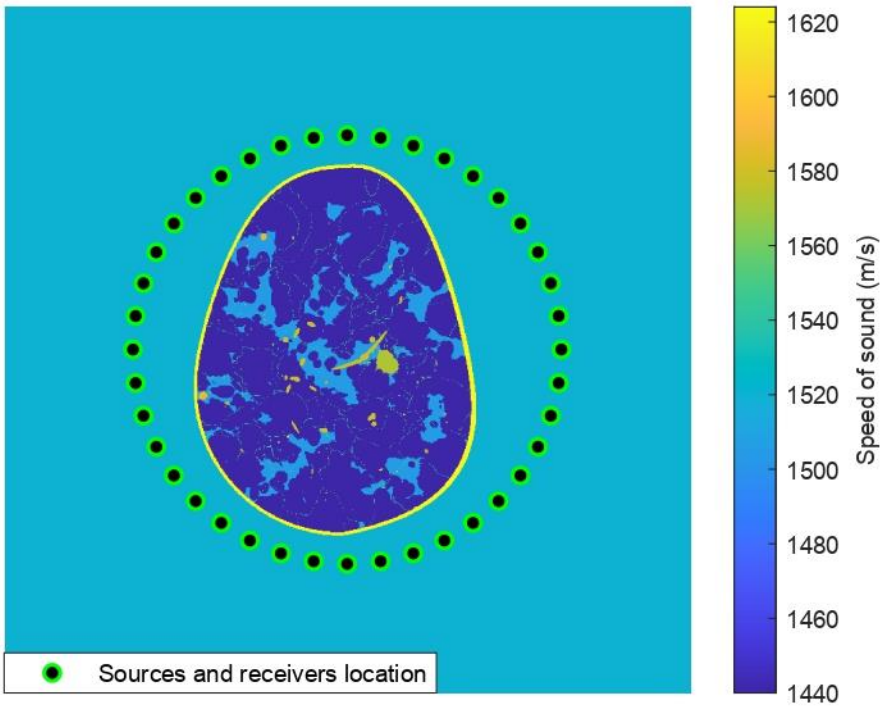

3.2.2 Acquisition of mammograms

Using the VICTRE software, mammography simulation was performed in three stages: compression, cropping, and X-ray imaging simulation. Figure 6 shows the flowchart of mammography simulation.

3.2.2.1 Compression and cropping. In this stage the uncompressed VBPs is loaded and a tetrahedral mesh is created around the volume. Then elasticity properties are assigned to the glandular and fatty tissues, the region containing the pectoral muscle was used as a limit in the

compression simulation. Subsequently, two compression paddles are simulated (one above and one below) in order to obtain a mammographic image with a craniocaudal view. Then the plates are moved towards each other until the desired compression is achieved. Finally, a displacement map is obtained and an interpolation is performed to determine the new position of each of the voxels of the sine without compressing in the compression process. Prior to the simulation of X-ray propagation, parts of the phantom that are not in the path of the X-ray source between the compression paddles are cropped.

3.2.2.2 X-ray imaging simulation. VICTRE includes a Monte Carlo MC-GPU X-ray transport simulation code. The Monte Carlo method is used to approximate complex mathematical expressions for stochastic or deterministic problems. X-rays are a form of ionizing electromagnetic radiation and are represented as the flow of a packet of energy, known as photons. Photon transport is often considered a stochastic problem due to the probabilistic nature of its behavior (Jacques et al., 1995). The MC-GPU code uses material files generated by the Penelope-2006 computer code system to simulate the photon propagation process in the different tissues. These files include information about the Rayleigh, Compton, Photoelectric, and Pair production interactions for different photon energies and the nominal densities of the material. These means of interaction are taken into account since they can degrade the image obtained. MC-GPU takes care of not only the photon transport, but also the X-ray source and detection network. The X-ray source has a focal spot with a nominal size of 0.3 mm and sampling on a Gaussian distribution is used to simulate the emission of the photons. In the detection network, binary random sampling is used to determine if the photons that arrive at the other side of the breast are absorbed or transmitted through a protective cover and an anti-scattering grid.

The parameters used for the mammography simulation were based on Badal A. et al. work depending of the BI-RADS 5.0 classifcation of each phantom (Badal et al., 2021). Finally, we obtained a set of 116 mammograms (one craneocaudal view from each of the 58 cases and 58 controls). with a pixel size of 85 μm.

Figure 6

Mammography simulation flowchart

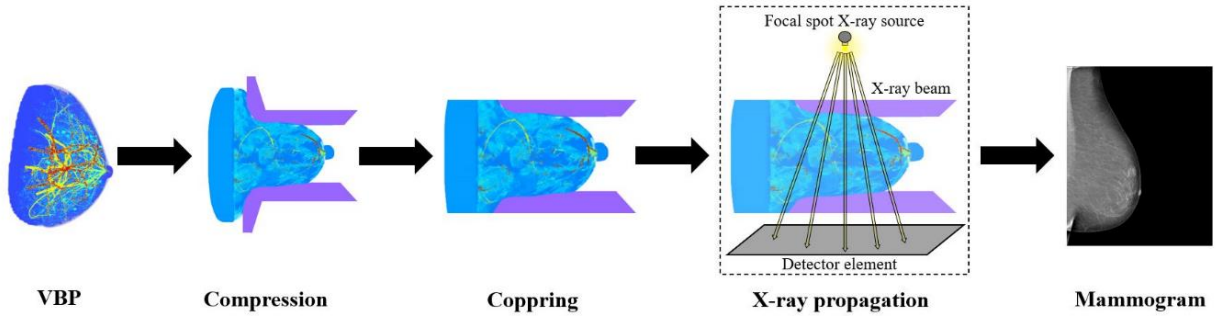

3.3 Lesion detection algorithm

In this work, we adopted a two-stage architecture for the detection of breast lesions that consist in radiomic feature extraction and classification. This classifier extracts radiomic features from reconstructed SOS images. Radiomic features can be divided into 5 main groups: statistical features, gray-level co-occurrence features, gray-level run-length, structural features and spectral features. We used the OpenBreast framework that extracts 33 radiomic features (Pertuz et al., 2019). In addition, we implemented a classifier based on radiomic features extracted from mammograms. As a result, we consider in total three classifiers: an SOS classifier based purely on radiomic features from USTC reconstructions, a mammographic classifier based on radiomic

features from mammograms, and a multimodal classifier that combines both USCT and mammographic features. Each of the classifiers is described below.

3.3.1 SOS classifier

For training the SOS image classifier, we use the slices in which the lesion is located in each VBP of the *cases group* and the corresponding slice of the same VBP in the *controls group* to train a multivariate logistic regressor. For testing, each slice of VBPs are entered in the trained logistic regressor, except some slices very close to pectoral wall and nipple were discarded since they do not include relevant information. Then, a score is obtained for each slice and this scores are the input of a *greedy* algorithm that computes a 3-tap moving average and selects the maximum score value of the sequence. Finally, we obtain a unique detection score at the breast level (see Figure 7).

Figure 7

SOS reconstruction classifier

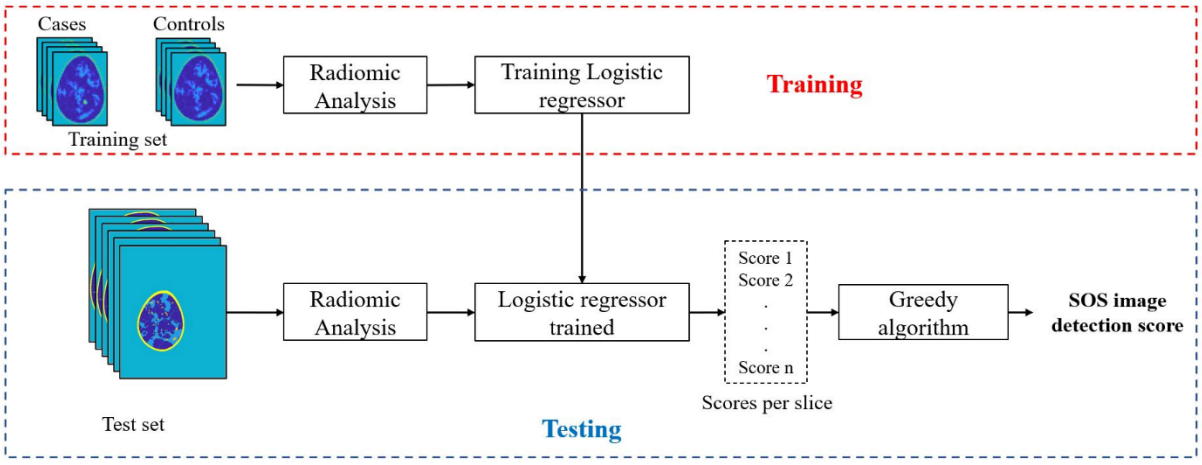

3.3.2 Mammographic classifier

The mammographic classifier was comprised by a radiomic analysis stage and a logistic regressor. Mammographic images are fed into the classifier which performs segmentation of the whole breast, then extracts the OpenBreast feature set from the segmented breast. The logistic regressor is trained with the features extracted from the mammograms of the training set. Then, the mammograms from the test set are entered into the grader and finally a detection score is obtained for each mammogram (see Figure 8).

Figure 8

Mammographic classifier

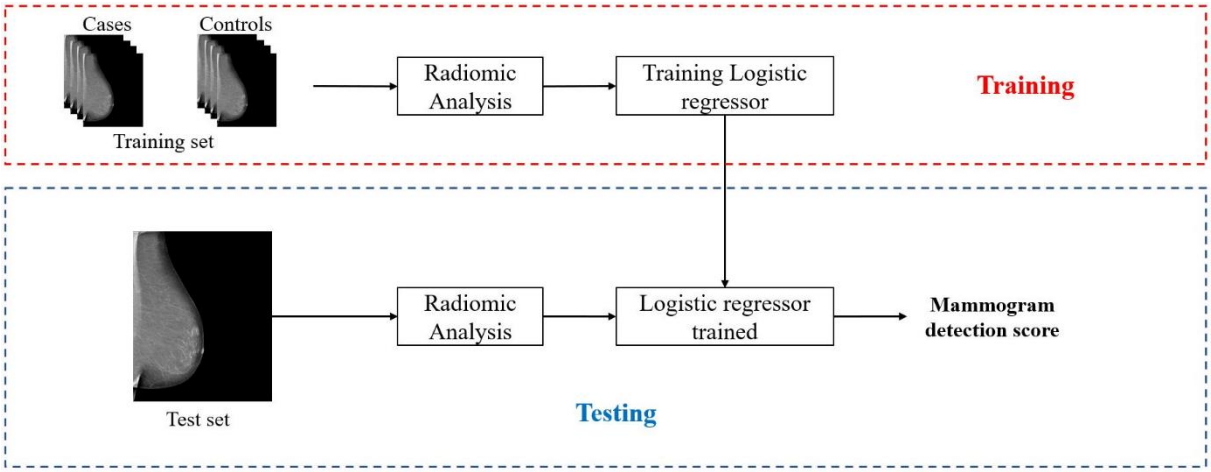

3.3.2 Multimodal classifier

The multimodal classifier uses the detection scores obtained for each phantom in the SOS classifier and the mammographic classifier. It then combines them in a logistic regressor to obtain a multimodal detection score. Figure 9 shows the flowchart of the multimodal classifier.

Figure 9

Multimodal classifier

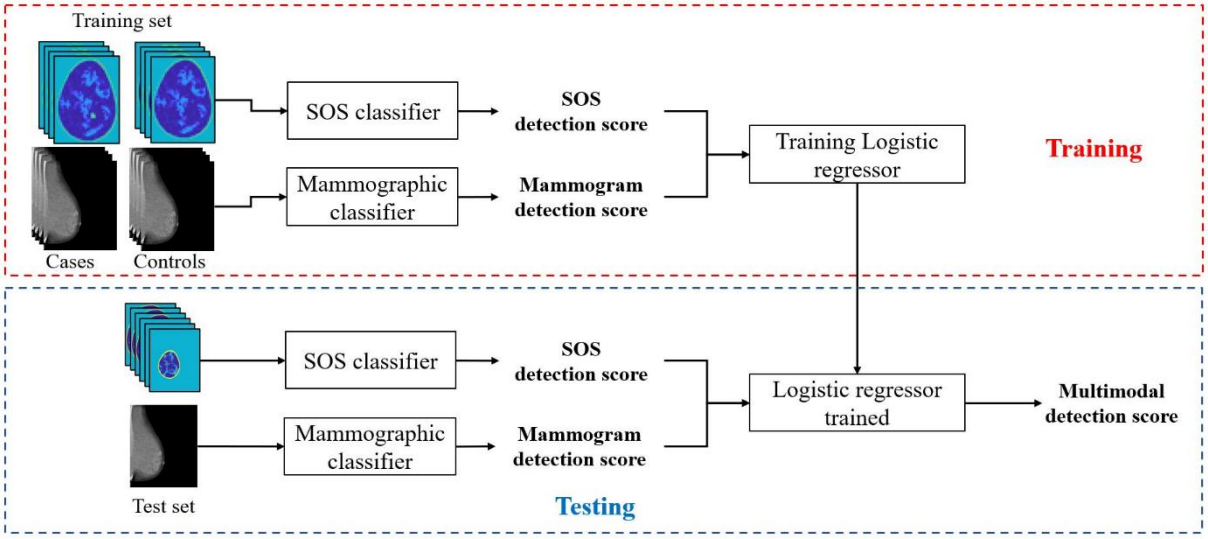

3.4 Performance measures

In this work we perform a Peak Signal to Noise Ratio (PSNR) analysis to establish the number of sources and receivers to use in the FWI simulation. To validate each of the classifiers presented in the previous section, a 5-fold cross-validation was implemented and their performance was measured in terms of area under the ROC curve (AUC). The ROC curve is a graphical representation of the trade-off between the sensitivity (the true positive rate) and the specificity (the true negative rate) of the model at different probability thresholds. Finally we use the Delong's test to compare the differences in AUCs among different experimental settings.

4. Experiments and results

The results of this work are divided in two. In the first part, we show the results of PSNR analysis carried out to select the number of sources and receivers in the FWI simulation. In the second part, we show the results in breast lesion detection.

4.1 FWI reconstruction

We performed a PSNR analysis on the reconstructions obtained from an SOS image corresponding to a 2D slice of a VBP. These reconstructions were obtained using 4 configurations in which the number of sources (N_s) and the number of receivers (N_r) were modified. Figure 10 shows the results of the SOS reconstruction using 100, 80, 60 and 40 for N_s and N_r.

Figure 10

Results of FWI simulation with different number of sources and receivers

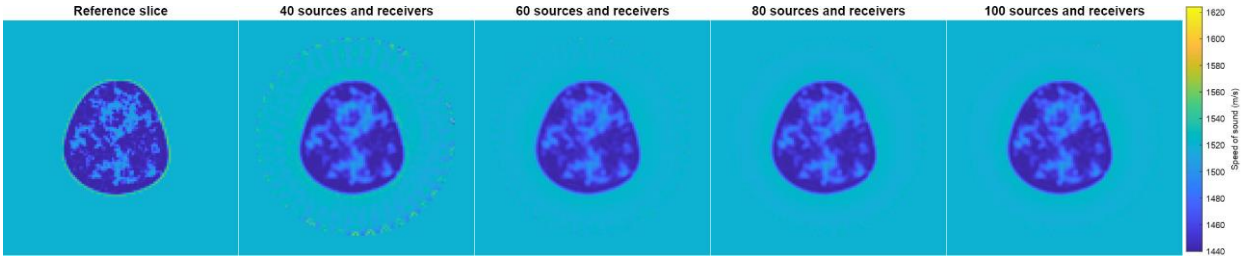

Note. (a) Reference slice, (b) NS = NR = 40 (PSNR = 54.73dB), (c) NS = NR = 60 (PSNR = 54.24dB), (d) NS = NR = 40 (PSNR = 54.59dB), (e) NS = NR = 40 (PSNR = 54.58dB).

4.2 Lesion detection

In this section we report the results of the use of each classifier presented in the section 3.3 Lesion detection algorithm). The performance results are presented in Table 3. The multimodal classifier outperformed the unimodal classifiers in terms of AUC. Differences in AUC were considered as statistically significant at the $p < 0.05$ level. The results of this test are shown in Table 4. According to the results of the Delong test, no significant differences were found between the SOS classifier and the mammographic classifier. While significant differences are found between the multimodal classifier and each of the unimodal classifiers.

Table 3

AUC of binary classification using the different classifiers

Classifier	**AUC (95% Confidence Interval)**
SOS classifier	0.81 (0.73 – 0.89)
Mammographic classifier	0.77 (0.68 – 0.86)
Multimodal classifier	**0.88 (0.82 – 0.95)**

Table 4

p-values resulting from Pairwise DeLong's test for the comparison of AUCs among different classifiers.

	Mammographic	**Multimodal**
SOS	0.535	**0.016**
Mammographic	-	**0.005**

5. Discussion

The results of FWI simulation for the SOS reconstructions show that by varying the number of sources and receptors in the ring configuration, no significant changes are observed in the internal region of the breast (see Figure 10). The differences in the PSNR measurements between each configuration are less than 1 dB. To streamline the simulation process and because the number of sources does not represent a significant change in the PSNR, 40 sources and receivers were used for the FWI simulation.

The results in the performance of the classifiers, for the detection of lesions in the breast, show that considering mammograms and SOS reconstructions, they outperform the classifiers that

use only one imaging modality. Although the SOS classifier showed superior results to the mammographic classifier in terms of AUC, no significant differences were found. This strengthens the added value of multimodal analysis for breast cancer diagnosis and detection tasks and is consistent with previous works (Sahiner et al., 2009) (Kelly et al., 2010). It should be clarified that in comparison to previous works that had the expert evaluation of radiologists, this work used radiomic analysis, a computerized automatic analysis method.

Figure 11 shows the distribution of scores using the classifiers presented in section 3.3 Lesion detection algorithm). The scores estimated using the multimodal classifier shows that it allows better discrimination between cases and controls, unlike the estimates using the SOS and mammographic classifiers.

Figure 11

Distribution of scores in cases and controls

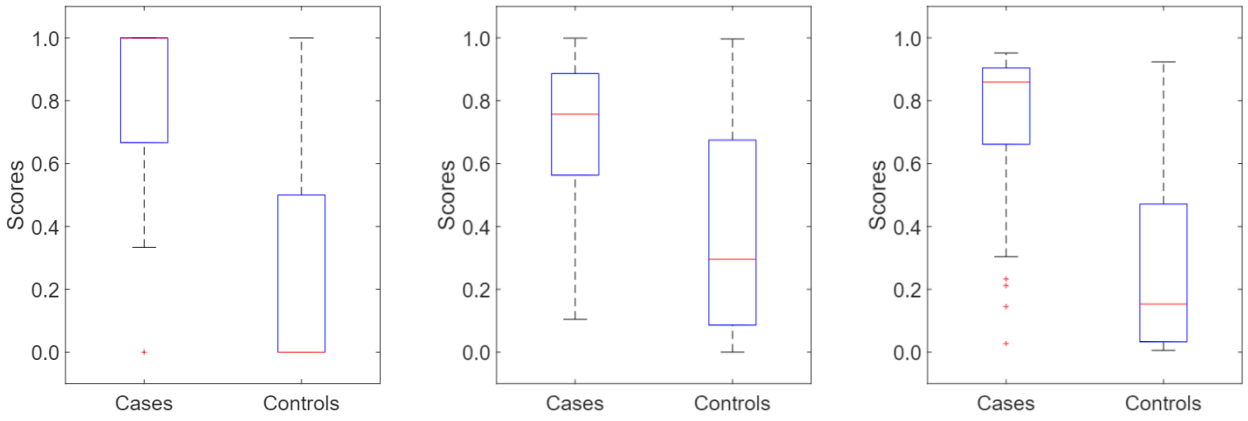

(a) (b) (c)

Note. Scores for: (a) SOS classifier, (b) mammographic classifier, and (c) multimodal classifier.

The development of new imaging modalities that allow the characterization of properties of the internal tissues of the breast can provide great added value to the computerized analysis of medical images. These new emerging imaging forms satisfy some limitations found in traditional imaging forms used in the clinical field, such as contrast-attenuation dependence and tissue overlap, being more prominent in dense breasts. The combination of these new imaging modalities in conjunction with computerized analysis methods they could be assisted diagnostic tools for radiologists. Although, it is important to recognize that it is not a replacement for the expertise and experience of radiologists, and that a combination of human and computerized analysis may provide better results.

In this work, the SOS image reconstructions were acquired with a pixel size of $2\,mm$. Future work should take into account the improvements in the FWI implementation for high-resolution reconstructions and the use of machine learning methods in it.

6. Conclusions

In this work, we evaluated the potential of multimodal radiomic analysis using mammography and ultrasound computed tomography using the reconstruction method called Full Wave-form Inversion for the task of breast lesion detection. For this purpose we carried out an in-silico experiment with a set of 116 virtual breast phantoms. We designed three classifiers: the first uses mammograms, the second uses the SOS reconstructions obtained from the FWI simulation, and the third uses the scores obtained on the other two classifiers. We compared the performance of the classifiers in terms of AUC, and found that performance using the multimodal classifier

outperforms classifiers using only one of the two imaging modalities. This work contributes in assessing the potential contribution in the adoption of USCT for breast cancer screening.

References

Abadi, E., Segars, W. P., Tsui, B. M., Kinahan, P. E., Bottenus, N., Frangi, A. F., ... & Samei, E. (2020). Virtual clinical trials in medical imaging: a review. Journal of Medical Imaging, 7(4), 042805-042805.

Africano, G., Arponen, O., Sassi, A., Karivaara-Mäkelä, M., Holli-Helenius, K., Rinta-Kiikka, I., ... & Pertuz, S. (2020, July). A comparison of regions of interest in parenchymal analysis for breast cancer risk assessment. In 2020 42nd Annual International Conference of the IEEE Engineering in Medicine & Biology Society (EMBC) (pp. 1136-1139). IEEE.

Amrane, M., Oukid, S., Gagaoua, I., & Ensari, T. (2018). Breast cancer classification using machine learning. In *2018 electric electronics, computer science, biomedical engineerings' meeting (EBBT)*, 1-4.

Arnold, M., Morgan, E., Rumgay, H., Mafra, A., Singh, D., Laversanne, M., ... & Soerjomataram, I. (2022). Current and future burden of breast cancer: Global statistics for 2020 and 2040. *The Breast*, 66, 15-23.

Badal, A., Sharma, D., Graff, C. G., Zeng, R., & Badano, A. (2021). Mammography and breast tomosynthesis simulator for virtual clinical trials. *Computer Physics Communications*, 261, 107779.

Badano, A., Graff, C. G., Badal, A., Sharma, D., Zeng, R., Samuelson, F. W., ... & Myers, K. J. (2018). Evaluation of digital breast tomosynthesis as replacement of full-field digital mammography using an in silico imaging trial. JAMA network open, 1(7), e185474-e185474.

Conti, A., Duggento, A., Indovina, I., Guerrisi, M., & Toschi, N. (2021). Radiomics in breast cancer classification and prediction. *Seminars in cancer biology*, 72, 238-250.

de Sisternes, L., Brankov, J. G., Zysk, A. M., Schmidt, R. A., Nishikawa, R. M., & Wernick, M. N. (2015). A computational model to generate simulated three-dimensional breast masses. *Medical physics*, 42(2), 1098-1118.

Fichtner, A., & Trampert, J. (2011). Hessian kernels of seismic data functionals based upon adjoint techniques. *Geophysical Journal International*, 185(2), 775-798.

Foster, F. S., Strban, M., & Austin, G. (1984). The ultrasound macroscope: initial studies of breast tissue. *Ultrasonic imaging*, 6(3), 243-261.

Gillies, R. J., & Schabath, M. B. (2020). Radiomics improves cancer screening and early detection. *Cancer Epidemiology, Biomarkers & Prevention*, 29(12), 2556-2567.

Guasch, L., Calderón Agudo, O., Tang, M. X., Nachev, P., & Warner, M. (2020). Full-waveform inversion imaging of the human brain. *NPJ digital medicine*, 3(1), 28.

Hasgall, P. A., Di Gennaro, F., Baumgartner, C., Neufeld, E., Lloyd, B., Gosselin, M. C., ... & Kuster, N. (2022). IT'IS Database for thermal and electromagnetic parameters of biological tissues. Version 4.0, 2018. *DOI: https://doi. org/10.13099/VIP21000-04-0. itis. swiss/database*.

Hernández, A., Miranda, D. A., & Pertuz, S. (2021). Algorithms and methods for computerized analysis of mammography images in breast cancer risk assessment. *Computer Methods and Programs in Biomedicine*, 212, 106443.

Jacques, S. L., & Wang, L. (1995). Monte Carlo modeling of light transport in tissues. In *Optical-thermal response of laser-irradiated tissue*, 73-100.

Kelly, K. M., Dean, J., Comulada, W. S., & Lee, S. J. (2010). Breast cancer detection using automated whole breast ultrasound and mammography in radiographically dense breasts. *European radiology*, 20, 734-742.

Kleman, C., Anwar, S., Liu, Z., Gong, J., Zhu, X., Yunker, A., ... & He, J. (2023). Full Waveform Inversion-Based Ultrasound Computed Tomography Acceleration Using Two-Dimensional Convolutional Neural Networks. *Journal of Nondestructive Evaluation, Diagnostics and Prognostics of Engineering Systems*, 6(4), 041004.

Klock, J. C., Iuanow, E., Malik, B., Obuchowski, N. A., Wiskin, J., & Lenox, M. (2016). Anatomy-correlated breast imaging and visual grading analysis using quantitative transmission ultrasound™. *International Journal of Biomedical Imaging*, 2016.

Lucka, F., Pérez-Liva, M., Treeby, B. E., & Cox, B. T. (2021). High resolution 3D ultrasonic breast imaging by time-domain full waveform inversion. *Inverse Problems*, 38(2), 025008.

Pérez-Liva, M., Herraiz, J. L., Udías, J. M., Miller, E., Cox, B. T., & Treeby, B. E. (2017). Time domain reconstruction of sound speed and attenuation in ultrasound computed tomography using full wave inversion. *The Journal of the Acoustical Society of America*, 141(3), 1595-1604.

Pertuz, S., Torres, G. F., Tamimi, R., & Kamarainen, J. (2019). Open framework for mammography-based breast cancer risk assessment. In *2019 IEEE EMBS International Conference on Biomedical & Health Informatics (BHI)*, 1-4.

Pisano, E. D., Gatsonis, C., Hendrick, E., Yaffe, M., Baum, J. K., Acharyya, S., ... & Rebner, M. (2005). Diagnostic performance of digital versus film mammography for breast-cancer screening. *New England Journal of Medicine*, 353(17), 1773-1783.

Ramirez, A. B., Abreo, S. A., & van Dongen, K. W. (2017). Selecting the number and location of sources and receivers for non-linear time-domain inversion. In *2017 IEEE International Ultrasonics Symposium (IUS)*, 1-3.

Ramirez, A. B., & van Dongen, K. W. (2016, September). Can sources and receivers be interchanged for imaging?. In *2016 IEEE International Ultrasonics Symposium (IUS)*, 1-4.

Robins, T., Camacho, J., Agudo, O. C., Herraiz, J. L., & Guasch, L. (2021). Deep-learning-driven full-waveform inversion for ultrasound breast imaging. *Sensors*, 21(13), 4570.

Sahiner, B., Chan, H. P., Hadjiiski, L. M., Roubidoux, M. A., Paramagul, C., Bailey, J. E., ... & Helvie, M. A. (2009). Multi-modality CADx: ROC study of the effect on radiologists' accuracy in characterizing breast masses on mammograms and 3D ultrasound images. Academic radiology, 16(7), 810-818.

Scheel, J. R., Lee, J. M., Sprague, B. L., Lee, C. I., & Lehman, C. D. (2015). Screening ultrasound as an adjunct to mammography in women with mammographically dense breasts. *American journal of obstetrics and gynecology*, 212(1), 9-17.

Sharma, D., Graff, C. G., Badal, A., Zeng, R., Sawant, P., Sengupta, A., ... & Badano, A. (2019). In silico imaging tools from the VICTRE clinical trial. Medical physics, 46(9), 3924-3928.

Schwardt, M., Köhn, D., Wunderlich, T., Wilken, D., Seeliger, M., Schmidts, T., ... & Rabbel, W. (2020). Characterization of silty to fine-sandy sediments with SH waves: Full waveform inversion in comparison with other geophysical methods. *Near Surface Geophysics*, 18(3), 217-248.

Sung, H., Ferlay, J., Siegel, R. L., Laversanne, M., Soerjomataram, I., Jemal, A., & Bray, F. (2021). Global cancer statistics 2020: GLOBOCAN estimates of incidence and mortality worldwide for 36 cancers in 185 countries. *CA: a cancer journal for clinicians*, 71(3), 209-249.

Taskin, U., Eikrem, K. S., Nævdal, G., Jakobsen, M., Verschuur, D. J., & Van Dongen, K. W. (2020). Ultrasound imaging of the brain using full-waveform inversion. In *2020 IEEE International Ultrasonics Symposium (IUS)*, 1-4.

Valdora, F., Houssami, N., Rossi, F., Calabrese, M., & Tagliafico, A. S. (2018). Rapid review: radiomics and breast cancer. *Breast cancer research and treatment*, 169, 217-229.

Van Timmeren, J. E., Cester, D., Tanadini-Lang, S., Alkadhi, H., & Baessler, B. (2020). Radiomics in medical imaging—"how-to" guide and critical reflection. *Insights into imaging*, 11(1), 1-16.

Wang, S., & Summers, R. M. (2012). Machine learning and radiology. *Medical image analysis*, 16(5), 933-951.

Yassin, N. I., Omran, S., El Houby, E. M., & Allam, H. (2018). Machine learning techniques for breast cancer computer aided diagnosis using different image modalities: A systematic review. *Computer methods and programs in biomedicine*, 156, 25-45.